Electron capture from Ar by fast protons: Capture from the M_1 subshell

Finn Grønne Kristensen and Erik Horsdal
Institute of Physics, University of Aarhus, DK-8000 Aarhus C, Denmark
(Received 11 February 1991)

The total cross section for the single-electron-capture reaction, $H^+ + Ar \rightarrow H + Ar^+\{(Ne)3s^1 3p^6; {}^2S\}$, has been measured at energies from 100 to 800 keV. The cross section is tentatively identified with the cross section for capture directly from the 3*s* single-electron orbital of Ar. A clear indication of a structure in the functional dependence of the cross section on energy is seen. It is suggested that the structure is caused by one of the two radial nodes of the 3*s* wave function. The cross sections for the simultaneous charge transfer and ionization reactions, $H^+ + Ar \rightarrow H^+ + Ar^{2+}\{(Ne)3s^1 3p^5; {}^1P$ and $ {}^3P\}$, $H^+ + Ar \rightarrow H + Ar^{3+}\{(Ne)3s^1 3p^4; {}^4P, {}^2D$, and $ {}^2P\}$, and $H^+ + Ar \rightarrow H + Ar^{4+}\{(Ne)3s^1 3p^3; {}^3D\}$, were also measured within the energy region 100–800 keV. The energy dependence of these cross sections is different from that found for the pure single-electron-capture reaction. The reason for this is, most likely, that the transfer and ionization reactions are influenced by electron capture from the *L* shell, followed by Coster-Kronig and Auger transitions. It is not known at present whether multielectron transitions due to dynamic electron correlation or multiple interactions with the projectile are important for the present collision systems. If so, the interpretation of the reactions will require a more thorough theoretical analysis.

I. INTRODUCTION

In theoretical treatments of electron capture in fast ion-atom collisions, it is most frequently assumed that the electron is captured directly from a specific single-particle orbital, and that the other electrons are inactive spectators [1]. Much experimental work on electron capture designed to test the fundamental understanding of the reaction has therefore been invested in determining cross sections for specific initial orbitals. This is done most directly by selecting true one-electron systems such as fully stripped ions colliding with atomic hydrogen or ground-state ions colliding with atoms in specific highly excited Rydberg states. Studies of this type are difficult due to the technical problems in producing and controlling sufficiently dense targets but, in spite of this, a number of important results have indeed emerged [2–6].

An equally important goal is to obtain cross sections for electron-capture reactions which lead to specific vacancy configurations of multielectron target atoms to explore the fundamental capture mechanisms in this complex environment and to test the basic single-particle assumption. The standard technique used for final states, with vacancies in inner orbitals, is to measure charge transfer in coincidence with the characteristic radiation from the decay of the inner-shell vacancy formed in the capture reaction. Most experiments of this type have concentrated on the *K* shell of the noble gases [7,8], but the *L* shell of Ar and the *M* shell of Kr have also been studied [8,9].

The technique enjoys widespread acceptance as yielding reliable single-particle cross sections for the orbitals or shells in question [1,10–14]. It has, however, been pointed out that multiple interactions between the projectile and the electrons of the target atom may lead to significant multielectron contributions to the measured cross section [15]. Such contributions are generally difficult to identify in total cross sections, but if they involve electrons from shells other than the one studied, they may reveal themselves in the energy dependence of the cross section [15]. Similarly, the cross section for a single-particle orbital with radial nodes exhibits characteristic structures at high energies, which may help in assessing the single-particle character of the reaction [16]. Unfortunately, these characteristics are probably not very different and never very distinct, so even when seen, they may easily be misinterpreted unless the experiments are supplemented by theoretical analysis.

In a recent survey of cross sections for ionization of atoms by protons, DuBois and Manson [17] found a structure in the energy dependence of the experimental cross section for the charge transfer and single-ionization reaction $H^+ + Ar \rightarrow H + Ar^+$. The authors could not find the origin of the structure and left it unexplained. This led to more experimental work [16] on the reaction to confirm the data and to extend the energy range to better cover the observed structure. It was also suggested [16] that the structure is a reflection of one or two of the radial nodes in the single-particle wave functions of 3*s* or 3*p* character that describe the M_1 and $M_{2,3}$ subshells of Ar, from which most of the capture takes place. In order to be able to better understand the nature of the observed structure, it is clearly desirable to have experimental cross sections also for the individual subshells.

This article describes a new experimental arrangement which has allowed us to measure the energy dependence of the cross section for the formation of singly charged Ar ions in the lowest excited spectroscopic ^2S state by electron capture. The final state of the ion is dominated by the electron configuration $\{(Ne)3s^1 3p^6\}$ which has a single hole in the M_1 subshell. The energy dependence of the measured electron-capture cross section most prob-

 ©1991 The American Physical Society

ably shows a real structure. We propose that the electron is captured directly from the $3s$ orbital of Ar, and that the structure is caused by one of the two radial nodes of the $3s$ wave function, but the structure could also be due to multielectron effects involving L-shell electrons [11], capture in the L shell followed by collisionally induced transfer of the L-shell vacancy to the M_1 subshell in a single collision, for example. These electrons, which have typical orbital speeds of about 7 a.u., are easily excited above the collision velocity of about 5 a.u. where the structure sets in. The structure would in this case be an example of what has been called a CESIME process [20] (coherent enhancement or suppression of independent multifermion events). The measured cross section is discussed in relation to other experimental cross sections for electron capture from Ar by protons, and it is compared with theoretical calculations for direct capture from the M_1 subshell.

The experimental arrangement also allowed measurement of cross sections for capturing one electron and at the same time ionizing other electrons, such that Ar^{2+}, Ar^{3+} and Ar^{4+} ions are formed in spectroscopic states dominated by configurations with one M_1-subshell vacancy and one to three $M_{2,3}$-subshell vacancies. These cross sections are of the same order of magnitude as the above pure single-electron-capture cross section, but they show a different energy dependence. This may be due to capture from the L shell with subsequent Coster-Kronig and Auger transitions. We support this interpretation by an estimate based on measured cross sections for electron capture from the L shell.

II. EXPERIMENTAL ARRANGEMENT

The experimental arrangement is shown in Fig. 1. A proton or deuteron beam from a 5-MV Van de Graaff accelerator with a rf ion source was momentum analyzed in a switching magnet, collimated by two sets of adjustable four-jaw slits, and charge-state purified in a second magnet before it was sent through a 1-cm-long gas cell with 1-mm-diam entrance and 2-mm-diam exit apertures. Cross sections for deuterons at impact energy E are taken to be equal to cross sections for protons at impact energy $E/2$. The Ar gas was leaked into the gas cell through a needle valve. The pressure in the gas cell was not measured directly but found indirectly to be close to 10^{-3} torr. The rest-gas pressure in the vacuum chambers was $(1-2)\times 10^{-6}$ torr. The final state of the Ar ions formed in the charge-transfer process was analyzed by a triple-coincidence technique. The three signals used are (A) formation of a hydrogen atom, (B) emission of a photon in the ultraviolet region, and (C) formation of an Ar ion in one of the four charge states from 1 to 4. The three branches and the coincidence technique are described below.

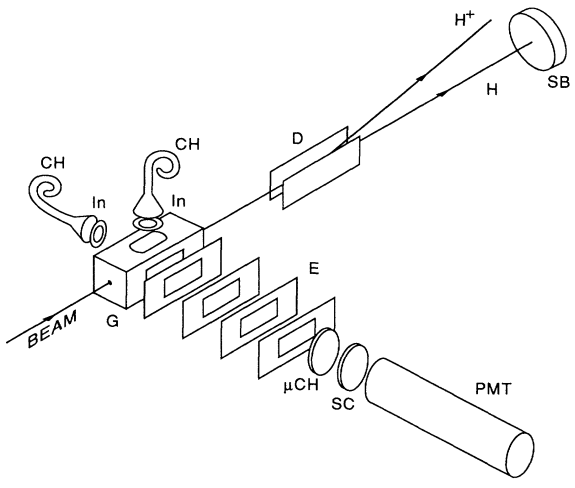

FIG. 1. Schematic diagram of the experimental arrangement. G, gas cell; D, electrostatic deflectors; SB, surface-barrier detector; CH, ceramic channeltrons; In, 1500-Å-thick In foils; E, recoil-ion extraction system; μCH, microchannel plate; SC, scintillator; and PMT, photo-multiplier tube.

A. Hydrogen-atom formation

The beam was charge-state analyzed after the gas cell by a set of electrostatic deflection plates, and the hydrogen atoms were detected by a Si surface-barrier detector. The energy sensitivity of this detector helped avoid slit scattering from the collimators and scattering off the entrance aperture of the gas cell when directing the beam through the apparatus.

B. uv-photon emission

Ultraviolet photons emitted from excited Ar ions or hydrogen atoms were detected by two secondary electron multipliers (Ceratron-E 1081B). The spectral region was defined by the uv-transmission window of 1500-Å-thick In foils placed in front of each multiplier. The transmission window extends from 750 to about 1000 Å. This spectral region includes the following transitions.

(1) $Ar^{0+}(3s^23p^6;{}^1S\text{-}nl\,[3/2])$ at 800–880 Å.
(2) $Ar^{+}(3s^23p^5;{}^2P\text{-}3s\,{}^13p^6;{}^2S)$ at 920–932 Å.
(3) $Ar^{2+}(3s^23p^4;{}^1S\text{-}3s\,{}^13p^5;{}^1P)$ at 769 Å.
(4) $Ar^{2+}(3s^23p^4;{}^3P\text{-}3s\,{}^13p^5;{}^3P)$ at 871–887 Å.
(5) $Ar^{3+}(3s^23p^3;{}^2P\text{-}3s\,{}^13p^4;{}^2P)$ at 754–761 Å.
(6) $Ar^{3+}(3s^23p^3;{}^2P\text{-}3s\,{}^13p^4;{}^2D)$ at 900–902 Å.
(7) $Ar^{3+}(3s^23p^3;{}^2D\text{-}3s\,{}^13p^4;{}^2D)$ at 801–802 Å.
(8) $Ar^{3+}(3s^23p^3;{}^4S\text{-}3s\,{}^13p^4;{}^4P)$ at 840–850 Å.
(9) $Ar^{4+}(3s^23p^2;{}^3P\text{-}3s\,{}^13p^3;{}^3D)$ at 822–836 Å.
(10) $H(1s\text{-}np;n\geq 3)$ at 913–1026 Å.

In the emission spectrum of Ar bombarded by fast protons or electrons [21], transitions 2–4 are strong, transitions 1 and 8 are weak, and transitions 5–7 and 9 are not seen. The effect of the Lyman series, transitions 10, is discussed in Sec. III.

The thickness and purity of the In foils used in the experiment were measured by Rutherford backscattering (RBS) of 2 MeV He^+ and by particle-induced x-ray Emission (PIXE) excited by 3-MeV protons. The RBS spectra gave thicknesses deviating only a few percent from the nominal value of 1500 Å and showed $\leq 4\%$ contaminations by C and O localized on the two surfaces. The amount of C clearly increased from a very low value with

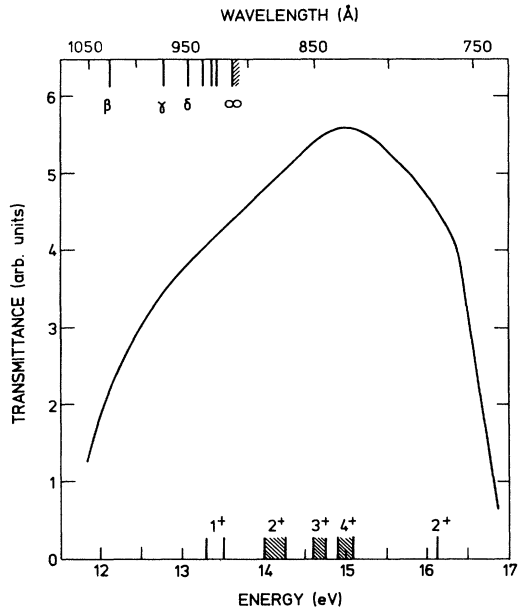

FIG. 2. Measured uv transmittance of a 1500-Å-thick In foil. The energies of uv photons from Ar ions in charge states $q^+=1^+-4^+$ are indicated on the lower scale. The wave-lengths of the Lyman series of H are indicated on the upper scale.

the beam exposure. The PIXE spectra showed tiny contaminations by Fe and Pb. The x rays from Fe could come from the vacuum vessel. The uv transmittance of the In foils was measured at the syncrotron-radiation facility BESSY in Berlin. The essential section of the transmittance spectrum is shown in Fig. 2.

C. Ar-ion formation

Ar ions formed in collisions with the fast protons were extracted from the gas cell by an electrostatic extraction system and directed onto a microchannel plate which, by a gain of about 10^3, converted the incoming flux of Ar ions into showers of electrons. These electrons were accelerated to 3 keV and then stopped in a plastic scintillator (NE 102) such that an energy of about $10^3\times 3$ keV$=3$ MeV was deposited for each extracted Ar ion. Finally, the photons from the scintillator were detected by a photomultiplier tube (Thorn EMI 9881B). This detection system is complicated, but, when combined with fast amplifiers, discriminators, and scalers, it is capable of counting at a random rate of 5×10^5 sec^{-1} for long periods of time without serious loss of gain. The current drawn from the microchannel plate was held at a modest level, with most of the gain for the total system coming from the photomultiplier tube which is designed for high counting rates over extended periods of time. The high counting rates are dictated by the large ratio between cross sections for ionization and for capture at high impact energies, which makes it necessary to detect a huge number of ions from pure ionization reactions for each ion produced in one of the capture reactions studied here. In spite of the high counting rates, the accumulation times were quite long. They ranged from 3–4 h at the lowest energies to nearly 60 h at the highest.

D. Coincidence technique

Fast amplifiers and constant fraction discriminators were used in all three detection branches. The fast timing signals from the uv-photon branch were used as start signals for two time-to-amplitude converters (TAC's), and the fast timing signals from the hydrogen-atom and the Ar-ion branches were used to stop each of the two TAC's. The output pulses from the two TAC's carrying the timing information were fed into two analog-to-digital converters and stored in three spectra. Two one-dimensional spectra showed coincidences between photons and hydrogen atoms and between photons and Ar ions, and one two-dimensional spectrum showed triple coincidences between the three branches.

III. EVALUATION OF CROSS SECTIONS

The electron-capture cross sections are evaluated from the numbers of real coincidences (double and triple) and the number of single photon counts, N.

A. Photon-Ar coincidences

A spectrum of coincidences between photons and Ar ions is shown in Fig. 3. The spectrum shows four peaks of real coincidences, one for each of the charge states 1^+-4^+, and an exponentially decreasing background of random coincidences. This exponential decrease is present because the TAC accepts only one stop pulse for each start. The decay constant of the exponential in Fig. 3 corresponds to a random stop rate of 5.75×10^5 sec^{-1}. The number of real coincidences for each charge-state component is determined by subtracting the random

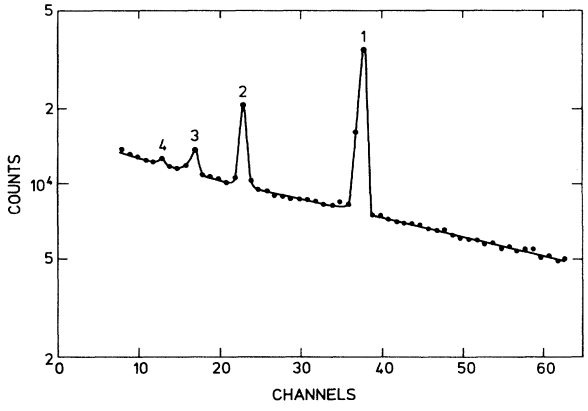

FIG. 3. Spectrum of coincidences between uv photons and Ar ions formed by 400-keV H^+ impact on Ar. Four peaks of real coincidences corresponding to Ar-ion charge states $q^+=1^+-4^+$ are seen on top of an exponentially decreasing background of random coincidences. The time range is about 2 μsec.

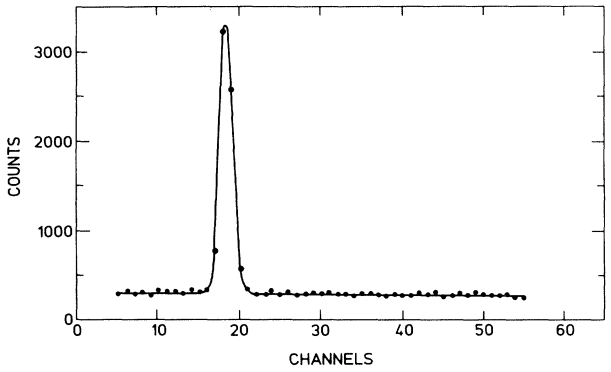

FIG. 4. Spectrum of coincidences between uv photons and hydrogen atoms for the same run as shown in Fig. 3. One peak of real coincidences is seen on top of a flat background of random coincidences. The time range is about 500 nsec.

background from each peak. These numbers are then corrected for the exponentially decreasing probability of detecting a real coincidence due to the large random stop rate. The corrected numbers are in the following referred to as $N_{c1}(q)$, where q refers to the charge state.

B. Photon-H coincidences

A spectrum of coincidences between photons and hydrogen atoms is shown in Fig. 4. The number of real photon-H coincidences corrected for the background of random coincidences is in the following referred to as N_{c2}.

C. Photon-Ar-H triple coincidences

A two-dimensional spectrum of triple coincidences is shown in Fig. 5. The spectrum has three peaks of triple coincidences, one for each of the charge states 1^+-3^+ of the Ar ion. Ridges of coincidences between two signals are also seen. The ridge of photon-H coincidences shows the same exponential decrease as seen in Fig. 3. Two ridges of photon-Ar coincidences for the charge states 1^+ and 2^+ are also seen, while the ridge for charge state 3^+ is buried in the random background. A third ridge of Ar-H coincidences extends from the peak of triple coincidences for charge state 1^+ towards the viewer. It is quite weak and formed when the TAC's are started by random photons and stopped by correlated Ar and H pulses. The two-dimensional spectra are analyzed in two steps. For each time segment along the photon-Ar axis, constituting a photon-H coincidence spectrum, the random coincidences are subtracted from the counts within the coincidence window, and the resulting number of real photon-H coincidences are plotted in a new spectrum (see Fig. 6). This spectrum is similar to that shown in Fig. 3. The real triple coincidences seen in the spectrum for charge states 1^+-5^+ were extracted and corrected for the decreasing detection probability, as explained earlier in this section in relation to Fig. 3. The numbers of real triple coincidences are in the following referred to as $N_{c3}(q)$.

D. Cross-section ratios

The number of uv photons detected during a run is given by

$$N = I\mu t\epsilon_1\Omega \sum_q \sigma(q)T(q) ,$$

where I is the beam intensity (particles/sec), μ is the target thickness (atoms per unit area perpendicular to the beam direction), t is the accumulation time, ϵ_1 is the detection efficiency of the channeltrons for uv radiation, Ω is the solid angle covered by the two channeltrons, q is the charge state of the Ar ion, $\sigma(q)$ is the effective cross

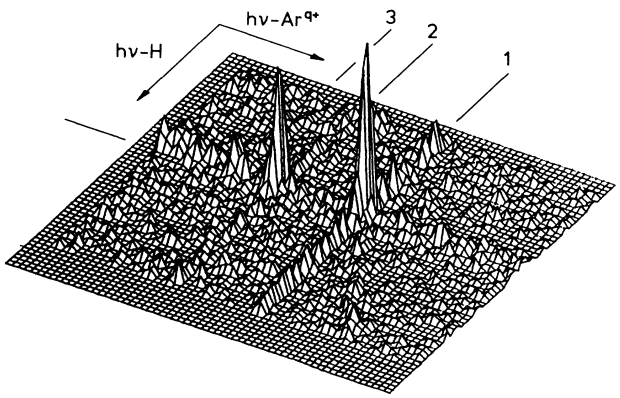

FIG. 5. Spectrum of triple coincidences between uv photons, Ar ions, and hydrogen atoms formed by 200-keV H^+ impact on Ar. Three peaks of real triple coincidences for the Ar-ion charge states $q^+=1^+-3^+$ are seen on top of ridges of real bilateral coincidences and a continuous background of random coincidences.

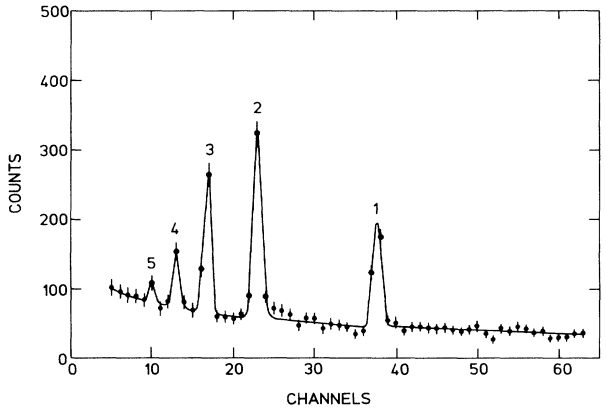

FIG. 6. Triple coincidences (from the same run as shown in Figs. 3 and 4) corrected for random coincidences and for the ridges of photon-Ar coincidences. Five peaks of real triple coincidences for the Ar-ion charge states $q^+=1^+-5^+$ are seen on top of an exponentially decreasing background of photon-H coincidences.

section for exciting the uv transitions listed in Sec. II for Ar ions in charge state q, and $T(q)$ is the transmission coefficient of the In foil at the wavelengths emitted by Ar ions in charge state q.

The number of real coincidences between photons and Ar ions in charge state q is given by

$$N_{c1}(q)=I\mu t\epsilon_1\epsilon_2\Omega\,\sigma(q)T(q)\ ,$$

where ϵ_2 is the extraction efficiency for the Ar ions.

The number of real photon-H coincidences is given by

$$N_{c2}=I\mu t\epsilon_1\Omega\sum_q\sigma_c(q)T(q)\ ,$$

where $\sigma_c(q=1-4)$ are the cross sections for exciting by electron capture the uv transitions listed in Sec. II.

The number of real triple coincidences for Ar ions in charge state q is given by

$$N_{c3}(q)=I\mu t\epsilon_1\epsilon_2\Omega\sigma_c(q)T(q)\ .$$

The following experimentally determined ratios were formed:

$$F_{c1}(q)=N_{c1}(q)\Big/\sum_q N_{c1}(q)$$
$$=[\sigma(q)T(q)]\Big/\left[\sum_q\sigma(q)T(q)\right]\ ,$$
$$R_{c2}=N_{c2}/N=\left[\sum_q\sigma_c(q)T(q)\right]\Big/\left[\sum_q\sigma(q)T(q)\right]\ ,$$
$$F_{c3}(q)=N_{c3}(q)\Big/\sum_q N_{c3}(q)$$
$$=[\sigma_c(q)T(q)]\Big/\left[\sum_q\sigma_c(q)T(q)\right]\ ,$$

and for each q combined to give ratios between the cross sections $\sigma_c(q)$ and $\sigma(q)$:

$$\sigma_c(q)/\sigma(q)=[F_{c3}(q)R_{c2}]/F_{c1}(q)\ .$$

These cross-section ratios are the basic experimental results of this work.

E. Cross sections

Absolute electron-capture cross sections $\sigma_c(q)$ are found from the above experimentally determined ratios by normalization to absolute excitation cross sections $\sigma(q)$. The cross section $\sigma(q=1)$ is known with an absolute uncertainty of ±25% in the energy region 150–1200 keV [22]. We extended this region downwards in energy to 100 keV by relative measurements in the energy region 100–300 keV and normalization above 150 keV (Fig. 7). The cross section $\sigma_c(q=1)$ for the electron-capture reaction

$$H^+ + Ar \rightarrow H + Ar^+\{(\ Ne\ )3s^1 3p^6, {}^2S\}$$

is obtained with an absolute uncertainty of ±25% in the energy region 100–800 keV when normalized to the above values of $\sigma(q=1)$. The statistical error depends on the number of real coincidences and real-to-random ratios for the different energies.

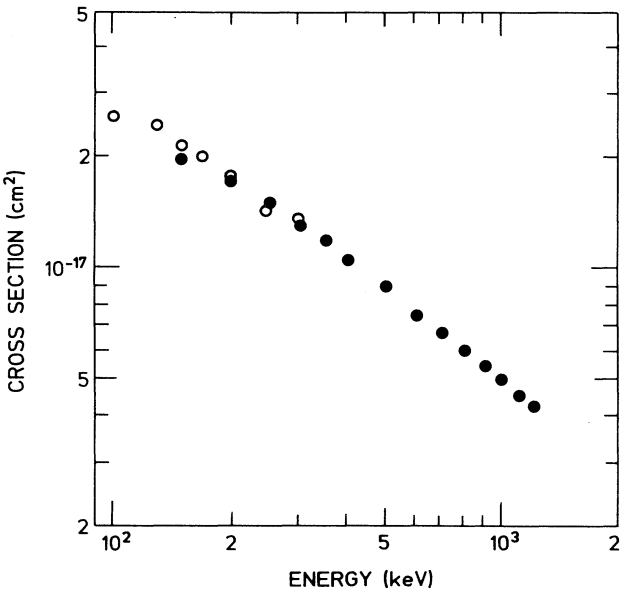

FIG. 7. Cross sections for excitation of $Ar^+\{(Ne)3s^1 3p^6; {}^2S\}$ by proton impact. Closed symbols from Ref. 22. Open symbols: present normalized results.

The excitation cross sections $\sigma(q)$ for $q=2-4$ were found from $\sigma(q=1)$ by the relation

$$\sigma(q)=[F_{c1}(q)/F_{c1}(q=1)][T(q=1)/T(q)]\sigma(q=1)\ ,$$

with the relative transmission $T(q=1)/T(q)$ taken from the measurements shown in Fig. 2. We find

$$T(q=1)/T(q=2)=0.87\pm0.03\ ,$$

$$T(q=1)/T(q=3)=0.77\pm0.03\ ,$$

and

$$T(q=1)/T(q=4)=0.75\pm0.03$$

where the uncertainty is due to the many spectral lines with different transmission coefficients that contribute to the cross sections for the different charge states.

When normalized in this way, the cross sections $\sigma_c(q=2)$, $\sigma_c(q=3)$, and $\sigma_c(q=4)$ for the electron-capture reactions

$$H^+Ar\rightarrow H+Ar^{2+}\{(Ne)3s^1 3p^5; {}^1P \text{ and } {}^3P\}$$

$$H^+Ar\rightarrow H+Ar^{3+}\{(Ne)3s^1 3p^4; {}^4P, {}^2D \text{ and } {}^2P\}$$

and

$$H+Ar\rightarrow H+Ar^{4+}\{(Ne)3s^1 3p^3; {}^3D\}$$

are obtained with an absolute uncertainty of the order of ±30% and statistical errors depending on counting statistics as for $\sigma_c(q=1)$.

The ratio R_{c2}, combined with the above cross sections $\sigma(q)$ and relative transmissions $T(q=1)/T(q)$,

leads to the weighted sum of cross sections $\sum_q \sigma_c(q)[T(q)/T(q=1)]$ which is approximately equal to $\sum_q \sigma_c(q)$. This cross section follows from the photon-H coincidences and can thus in practice be measured in a broader range of energies than can the individual cross sections $\sigma_c(q)$ which depend on triple coincidences. The cross section is included in the experimental results, but it is of secondary interest only.

F. Lyman series

In the above discussion, we assumed that the uv photons come exclusively from the decay of excited Ar ions, but some may also be emitted from fast hydrogen atoms formed in excited states. Such photons may result in real triple and double coincidences which cannot be distinguished from coincidences due to radiation from Ar ions. We now give a realistic estimate of the relative contribution to the measured triple coincidences from photons belonging to the Lyman series of hydrogen. The relative contribution to the photon-H coincidences is of the same order of magnitude. The photon-Ar coincidences are influenced only very little by the Lyman series due to the small ratio between electron capture and excitation cross sections at the present energies.

The Ly α transition at 1216 Å is absorbed by the In foils, but all the other members of the series lie within the transmission window. The number of triple coincidences from this source in a given run is

$$N(H)=I\mu t\epsilon_1\epsilon_2\Omega\sum_n \sigma^c(n)T(n)P(n)\ ,$$

where $\sigma^c(n)$ is the cross section for electron capture from Ar to a p state of hydrogen with main quantum number n, $T(n)$ is the transmission coefficient of the In foil for the Lyman radiation from this state, and $P(n)$ is the probability that the hydrogen atom radiates directly to the ground state within the gas cell. These triple coincidences are distributed on the various charge states q of the Ar ions.

For the relative contribution of the Lyman series to the triple coincidences with Ar ions in charge state q, one finds

$$R(q)=[N(H)F(q)]/N_{c3}(q)$$
$$=\left[\left[\sum_n \sigma^c(n)T(n)P(n)\right]\Big/[\sigma_c(q)T(q)]\right]F(q)\ ,$$

where $F(q)$ is the fraction of Ar ions left in charge state q as a result of the excitation of the Lyman radiation by electron capture.

A realistic estimate of $\sigma^c(n)$ is $\sigma^c(n)=(3/n)^3\sigma^c$, where σ^c is the experimental cross section for capture to the $3p$ state [23]. The probability $P(n)=1-\exp[-A(n)\tau]$, where $A(n)$ is the transition probability to the ground state [24], and $\tau=L/2v$ is the average time spent by the excited projectile in the gas cell. The quantities L and v are the length of the gas cell and the beam velocity, respectively. The factors $T(n)/T(q)$ are read from Fig. 2. The fractions $F(q)$ are approximated by measured fractions [25] for total electron capture by protons from Ar.

TABLE I. Relative contributions, $R(q)$, of Lyman series to the triple coincidences for the four charge states $q=1$–4 of the Ar ion.

E (keV)	$R(q)$(%) $q=1$	$q=2$	$q=3$	$q=4$
100	2.92	1.08	0.71	
200	1.90	0.68	0.24	
400	0.34	0.23	0.16	0.16
800	0.24	0.17	0.13	0.12

With these values, we find the $R(q)$ values listed in Table I. The main uncertainty of these values comes from the cross section σ^c which has a quoted [23] systematic error of no more than 16.5%. The contributions are so small that they can be neglected in the discussion of the results.

IV. EXPERIMENTAL RESULTS AND DISCUSSION

In an independent-electron picture, the measured electron-capture cross section $\sigma_c(q=1)$ refers to a specific capture reaction, in which an Ar^+ ion with electron configuration $(Ne)3^13p^6$ is formed. This final state is not necessarily formed only in one-electron capture directly from the $3s$ state of Ar, with the rest of the electrons being inactive spectators, but may result from many reaction channels involving more than one active electron. One possibility is a two-electron reaction, in which an L-shell electron is captured, and an electron from the M_1 subshell is simultaneously transferred to fill the L-shell vacancy formed in the charge-transfer reaction. Another possibility is capture of a $3p$ electron, with simultaneous excitation of the hole to the $3s$ state. Multielectron processes of this type have been treated quite generally by a coupled-channels method with independent electrons described by wave functions in the form of Slater determinants [26]. Detailed calculations following such lines are needed for assessing the relative importance of the various coherent reaction channels, but even further sophistication will be necessary if electron correlation is important. The state of the Ar^+ ion that we are discussing here is the lowest-excited ^2S state. This state is dominated by the electron configuration $(Ne)3s^13p^6$, but other configurations contribute as well. The most important of these configurations [27] is $(Ne)3s^23p^43d^1$. Another possible reaction channel (involving static correlation or configuration interaction in the Ar^+ ion) is thus simultaneous capture of one $3p$ electron and $3p$-to-$3d$ excitation of another. If the excitation of the various multiply excited states of the Ar^+ ion is allowed to take place not only by interactions with the projectile field but also by electron-electron interactions during the collision, then dynamic correlation is involved [18,19]. This is quite difficult to include in practical calculations [20].

In the following, we take the simplest approach and interpret $\sigma_c(q=1)$ as the cross section for capture directly from the $3s$ orbital (or the M_1 subshell) of the Ar atom

and denote it $\sigma_c(M_1)$. The cross section is shown as a function of energy in Fig. 8. The figure also shows previously published [16] cross sections for the reaction $H^+ + Ar \rightarrow H + Ar^+$, in which one electron is captured and the Ar atom is left singly ionized. These quantities [called $\sigma_c(M)$] are interpreted as cross sections for capture directly from the M shell because capture from the K or L shells is followed by vacancy cascades leading to multiply charged Ar ions in most cases, but again we cannot exclude the possibility that multielectron reactions involving inner shells contribute significantly to the measured cross section.

The cross sections $\sigma_c(M)$ and $\sigma_c(M_1)$ both decrease rapidly with increasing energy in the present energy range as one would expect. The cross section $\sigma_c(M)$ shows a structure in the energy dependence near 450 keV which was discussed earlier [16] on the assumption that $\sigma_c(M)$ represents the cross section for capture directly from the $3s$ or the $3p$ orbital of Ar. It was suggested that the structure is due to one or two of the radial nodes of the $3s$ and $3p$ wave functions. A similar, although smaller, structure may be present in $\sigma_c(M_1)$ between 500 and 600 keV. This is perhaps seen more clearly in Fig. 9 where $\sigma_c(M_1)E^{3.75}$ is plotted as a function of energy E on linear scales. The cross section seems to decrease nearly as $E^{-3.75}$ in the energy region 130–500 keV and then suddenly somewhat slower in the region 600–800 keV. One of the two radial nodes in the $3s$ wave function of Ar would lead to a structure near 530 keV,[16] in almost perfect agreement with the experiment finding.

Calculations in the Oppenheimer-Brinkman-Kramers (OBK) approximation, in the two-state two-center atomic-expansion (TSAE) method [28], and in the screened boundary-corrected 1st-Born (SB1B) approximation [29] for capture directly from the $3s$ orbital are also shown in Fig. 8. The OBK cross section was calculated on the basis of accurate Compton profiles [30] for the $3s$ wave function of Ar. The connection is the following:

$$\sigma = \frac{32\pi^2}{v^2}\left[\frac{J(q_{\min})}{(p_{\min}^2+1)^2} - 4\int_{q_{\min}}^{\infty}\frac{qJ(q)}{(p^2+1)^3}dq\right],$$

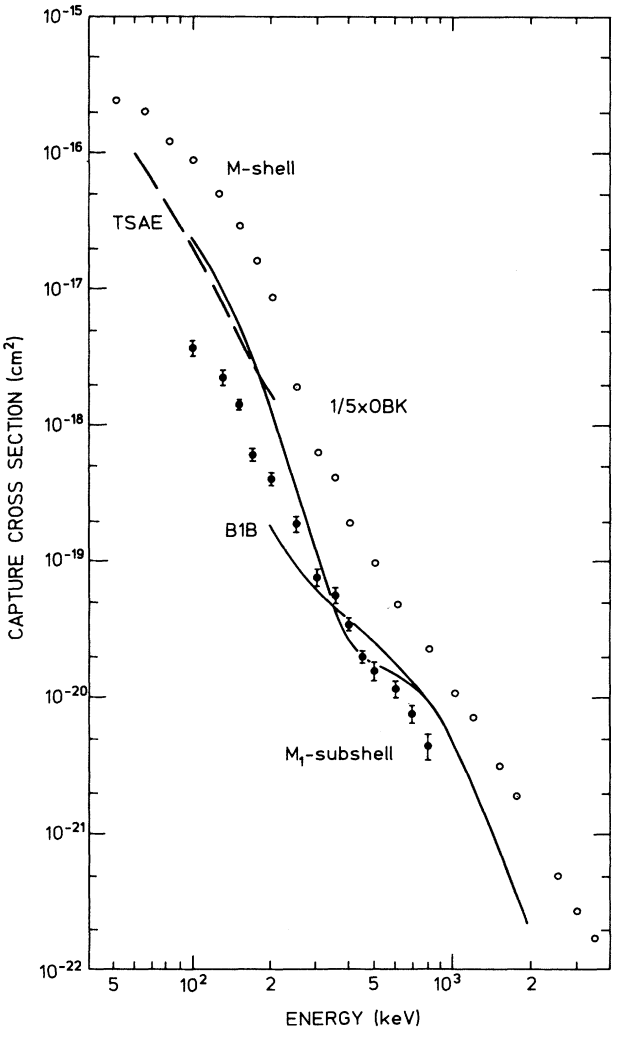

FIG. 8. Cross sections for forming Ar^+ ions (M shell, open symbols) and $Ar^+\{(Ne)3s^13p^6;^2S\}$ ions (M_1 subshell, closed symbols) in electron capture by protons. The full-drawn curves show calculations in the SB1B approximation [29] and in the OBK approximation (reduced by a factor of 5, see text). The broken line shows calculations in the TSAE approximation [28].

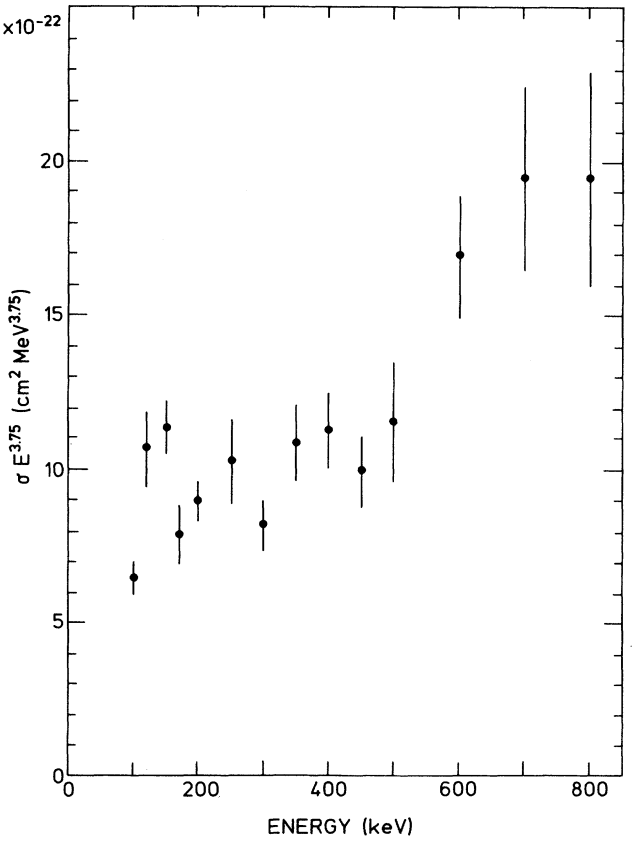

FIG. 9. M_1-subshell cross sections from Fig. 8 multiplied by energy to the power 3.75.

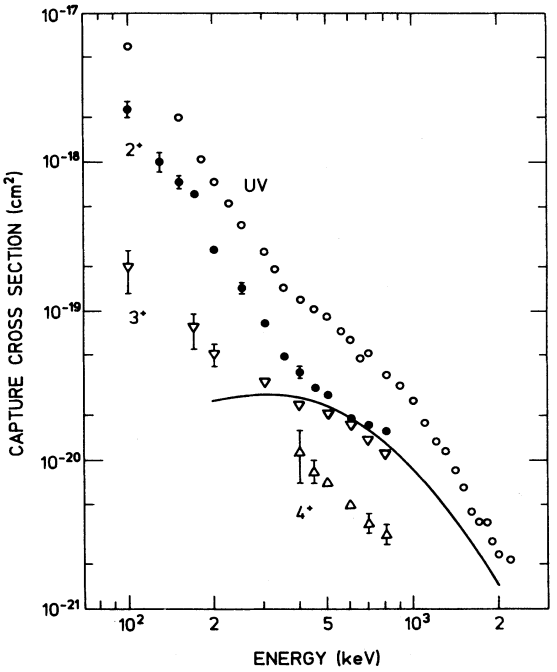

FIG. 10. Cross sections for forming $Ar^{2+}\{(Ne)3s^13p^5;{}^1P$ and $^3P\}$, $(2^+,\bullet)$; $Ar^{3+}\{(Ne)3s^13p^4;{}^4P,{}^2D$, and $^2P\}$, $(3^+,\nabla)$; and $Ar^{4+}\{(Ne)3s^13p^3;{}^3D\}$ $(4^+,\triangle)$ in electron capture by protons. Full-drawn curve, empirical estimate of cross section 2^+. Total cross section for producing uv radiation (uv,○) in electron capture by protons.

where σ is the OBK cross section [31] for a single $3s$ electron, $J(q)$ is the Compton profile, $q_{\min}=v/2-\Delta E/v$ where v is the collision velocity and ΔE the energy defect of the process, $p^2=q^2+2\Delta E$, and $p^2_{\min}=q^2_{\min}+2\Delta E$. The OBK cross section for the M_1 subshell $(=2\sigma)$ has (arbitrarily) been divided by five to fit the SB1B cross section at high energies. The TSAE and the SB1B results shown in Fig. 8 are, just like the OBK results, based on accurate single-particle wave functions for the $3s$ state.

The SB1B cross section is seen (Fig. 8) to be of the right order of magnitude when compared to the experimental cross section $\sigma_c(M_1)$, and both the OBK and the SB1B cross sections show a structure due to the innermost radial node of the $3s$ momentum-space wave function, but the theoretical structures are much stronger than the experimental one. Higher-order contributions to the capture cross section have the effect of smearing out the structure predicted by the OBK approximation [32], but no theoretical calculation going past the lowest order is available for comparison at present. The TSAE cross section shows approximately the same energy dependence as the experimental cross section but lies about a factor of 4 higher in the narrow energy range where a comparison can be made.

The cross sections $\sigma_c(q=2)$, $\sigma_c(q=3)$, and $\sigma_c(q=4)$ for (in an independent-electron picture) forming Ar ions with one M_1-subshell vacancy and one, two, and three M_{23}-subshell vacancies, respectively, by electron capture are shown as functions of projectile energy in Fig. 10. The figure also includes approximate values of the cross section $\sigma_c(\text{uv})=\sum_q\sigma_c(q)$ for producing uv radiation in the interval 750–1000 Å by electron capture. This cross section does not require triple coincidences. It could therefore be measured in a broader range of energies than could the other cross sections.

The cross section $\sigma_c(q=2)$ is about a factor of 2 smaller than $\sigma_c(M_1)$ for $E=100$–250 keV. At higher energies, $\sigma_c(q=2)$ decreases much less rapidly than does $\sigma_c(M_1)$ and at 800 keV lies a factor of 3.5 above $\sigma_c(M_1)$. The ratios between the cross sections $\sigma_c(q=2)$, $\sigma_c(q=3)$, and $\sigma_c(q=4)$ are approximately constant at high energies. This indicates that there is a common basic mechanism behind these cross sections at high energies, and that this mechanism is different from the one governing $\sigma_c(M_1)$. We suggest that the basic mechanism is electron capture from the L shell of Ar with subsequent Auger or Coster-Kronig transitions. This is substantiated to some degree by an estimate of the cross section $\sigma_c(q=2)$ based on this assumption. Experimental capture cross sections for the full L shell $\sigma_c(L)$ were used, and it was assumed that only the $L_{2,3}$ subshell contributes to $\sigma_c(q=2)$ because L_1-subshell vacancies lead to charge state 3 or higher in nearly all cases. It was further assumed that the $L_{2,3}$ subshell contributes to the total L-shell cross section according to its statistical weight. The branching ratio of 16% for the $L_{2,3}M_1M_{2,3}$ Auger transition populating the final state was taken from experimental Auger spectra [33]. With these assumptions, one finds

$$\sigma_c(q=2)=\tfrac{3}{4}\sigma_c(L)0.16=0.12\sigma_c(L)\ .$$

This empirical estimate of $\sigma_c(q=2)$ is shown in Fig. 10 as a full-drawn curve. It shows very clearly that the high-energy behavior of $\sigma_c(q=2)$ can be explained by the proposed mechanism. The cross sections $\sigma_c(q=3)$ and $\sigma_c(q=4)$ depend on capture from both the L_1 and $L_{2,3}$ subshells and possibly also on further ionization of the $M_{2,3}$ subshell due to shakeoff or direct ionization, but this would still give an energy dependence very similar to the one estimated for $\sigma_c(q=2)$.

The cross section $\sigma_c(\text{uv})$ deviates very little from $\sum_q\sigma_c(q)$ at energies below 300 keV, and at energies in the region 400–800 keV by about 20% only $[\sigma_c(\text{uv})\geq\sum_q\sigma_c(q)]$. The difference is due to the different transmissions of the In foils for the uv lines contributing to $\sigma_c(\text{uv})$. A comparison between the estimate of $\sigma_c(q=2)$ and $\sigma_c(\text{uv})$ indicates that the behavior of $\sigma_c(\text{uv})$ [and $\sigma_c(q=2-4)$] is governed by capture from the L shell at energies up to at least 2 MeV.

V. SUMMARY

Cross sections for populating specific excited states of Ar ions in charge states 1–4 in electron-capture reactions by fast protons have been measured. In an independent-electron picture, all the excited states have one $3s$ vacancy and from zero to three $3p$ vacancies. The cross sections are interpreted in terms of direct capture from the $3s$ orbital or capture from the L shell, followed by Coster-Kronig and Auger transitions. Theoretical

analysis is needed to determine whether this interpretation represents an oversimplification.

ACKNOWLEDGMENTS

The authors would like to express their gratitude to F. Decker and J. Eichler for discussions and communication of unpublished theoretical results, to K.-H. Schartner for unpublished uv spectra for *p*-Ar, to N. Hertel for PIXE analysis, to F. Lyckegaard for making the In foils, and to D. Adams and D. Batchelor for invaluable support in connection with the measurements at BESSY.

[1] D. H. Jakubassa-Amundsen, Int. J. Mod. Phys. **4**, 769 (1989).
[2] T.V. Goffe, M. B. Shah, and H. B. Gilbody, J. Phys. B **12**, 3763 (1979).
[3] P. Hvelplund and A. Andersen, Phys. Scr. **26**, 375 (1982).
[4] R. A. Phaneuf, I. Alvarez, F.W. Meyer, and D. H. Crandall, Phys. Rev. A **26**, 1892 (1982).
[5] W. Schwab, G. B. Baptista, E. Justiniano, R. Schuch, H. Vogt, and E. W. Weber, J. Phys. B **20**, 2825 (1987).
[6] K. B. MacAdam, in *Atomic Physics 12,* edited by J. Zorn and R. L. Lewis (AIP, New York, 1991), p.298.
[7] E. Horsdal-Pedersen, C. L. Cocke, J. L. Rasmussen, S. L. Vaghese, and W. Waggoner, J. Phys. B **16**, 1799 (1983).
[8] M. Rødbro, E. Horsdal-Pedersen, C. L. Cocke, and J. R. Macdonald, Phys. Rev. A **19**, 1936 (1979).
[9] S. Andriamonje, J. F. Chemin, J. Rotourier, B. Saboya, J. N. Scheurer, Dz. Belkic, R. Gayet, A. Salin, H. Laurent, and J. P. Schapira, J. Phys. (Paris) **46**, 349 (1985).
[10] L. Kocbach, J. Phys. B **13**, L665 (1980).
[11] Dz. Belkic, R. Gayet, J. Hanssen, and A. Salin, J. Phys. B **19**, 2945 (1986).
[12] F. Decker and J. Eichler, Phys. Rev. A **39**, 1530 (1989).
[13] H. Marxer and J. S. Briggs, Z. Phys. D **13**, 75 (1989).
[14] K. Taulbjerg, R. O. Barrachina, and J. H. Macek, Phys. Rev. A **41**, 207 (1990).
[15] A. L. Ford, J. F. Reading, and R. L. Becker, Phys. Rev. A **23**, 510 (1981); R. L. Becker, A. L. Ford, and J. F. Reading, J. Phys. B **13**, 4059 (1980).
[16] E. Horsdal-Pedersen and J. P. Giese, Phys. Rev. A **41**, 4831 (1990).
[17] R. D. DuBois and S. T. Manson, Phys. Rev. A **35**, 2007 (1987).
[18] J. H. McGuire, Phys. Rev. A **36**, 1114 (1987).
[19] N. Stolterfoht, Phys. Scr. **42**, 192 (1990).
[20] J. F. Reading and A. L. Ford, Comments At. Mol. Phys. **23**, 301 (1990).
[21] K.-H. Schartner, B. Kraus, W. Pöffel, and K. Reymann, Nucl. Instrum. Methods B **27**, 519 (1987); K.-H. Schartner (private communication).
[22] R. Hippler and K.-H. Schartner, J. Phys. B **7**, 1167 (1974).
[23] J. C. Ford and E. W. Thomas, Phys. Rev. A **5**, 1694 (1972).
[24] H. Bethe and E. E. Salpeter, *Quantum Mechanics of One- and Two-Electron Systems* (Springer, Berlin, 1975).
[25] E. Horsdal-Pedersen and L. Larsen, J. Phys. B **12**, 4085 (1979).
[26] R. L. Becker, A. L. Ford, and J. F. Reading, Phys. Rev. A **29**, 3111 (1984).
[27] B. F. J. Luyken, Physica **60**, 432 (1972).
[28] C. D. Lin and L. N. Tunnel, J. Phys. **12**, L485 (1979).
[29] F. Decker and J. Eichler (private communication); theoretical details regarding in particular the effect of screening may be found in Ref. [12]; D. P. Dewangan and K. Eichler, Comments At. Mol. Phys. **21**, 1 (1987).
[30] F. Biggs, C. B. Mendelsohn, and J. B. Mann, At. Data Nucl. Data Tables **16**, 201 (1975).
[31] M. R. C. McDowell and J. P. Coleman, *Introduction to the Theory of Ion-Atom Collisions* (North-Holland, Amsterdam, 1970), Chap. 8.
[32] D. H. Jakubassa-Amundsen, J. Phys. B **14**, 2747 (1981).
[33] W. Mehlhorn and D. Stalherm, Z. Phys. **217**, 294 (1968).